

Daily Hurricane Variability Inferred from GOES Infrared Imagery

JAMES P. KOSSIN

Cooperative Institute for Research in the Atmosphere, Colorado State University, Fort Collins, Colorado

(Manuscript received 9 November 2001, in final form 7 February 2002)

ABSTRACT

Using the National Environmental Satellite, Data, and Information Service–Cooperative Institute for Research in the Atmosphere (NESDIS–CIIRA) tropical cyclone infrared (IR) imagery archive, combined with best track storm center fix information, a coherent depiction of the temporal and azimuthally averaged spatial structure of hurricane cloudiness is demonstrated. The diurnal oscillation of areal extent of the hurricane cirrus canopy, as documented in a number of previous studies, is clearly identified but often found to vanish near the convective region of the hurricane eyewall. While a significant diurnal oscillation is generally absent near the storm center, a powerful and highly significant semidiurnal oscillation is sometimes revealed in that region. This result intimates that convection near the center of tropical storms and hurricanes may not be diurnally forced, but might, at times, be semidiurnally forced. A highly significant semidiurnal oscillation is also often found in the near environment beyond the edge of the hurricane cirrus canopy. The phase of the semidiurnal oscillations in both the central convective region and the region beyond the canopy remains relatively fixed during the lifetime of each storm and is not found to vary much between individual storms. This fixed phase near the central convective region insinuates a mechanistic link between hurricane central convection and the semidiurnal atmospheric thermal tide S_2 .

Two hypotheses are constructed. The first is offered to explain the diurnal oscillation of the canopy in the absence of a diurnal oscillation of the convective regions. The hypothesized mechanism is based on the radial variation of nighttime net radiational cooling and subsidence. The second hypothesis is offered to explain the semidiurnal oscillation near the central convective region, and is based on the possible presence of a semidiurnal oscillation of local lapse rates associated with S_2 .

1. Introduction

As a typical tropical storm develops, vigorous convection near the vortex center penetrates vertically to the tropopause and spreads radially outward to form a cirriform canopy (Merritt and Wexler 1967). The canopy generally exists throughout the lifetime of the storm, provided that convection is maintained near the storm center and, to a lesser extent, within the surrounding spiral bands. A number of previous studies using geostationary IR satellite imagery have considered the temporal evolution of tropical cyclone cloudiness in various ocean basins, and have revealed a strong diurnal (24 h period) cycle in the horizontal areal extent of the canopies above the storms (Browner et al. 1977; Muramatsu 1983; Lajoie and Butterworth 1984). The specific features of this well-documented diurnal oscillation vary somewhat between each study, particularly in the phase of the oscillation (i.e., the time of maximum areal extent). The interpretation of the diurnal oscillation of tropical cyclone cirrus canopies has conventionally rest-

ed on the assumption that it is predominantly forced by a diurnal oscillation in deep convection near the storm center (e.g., Browner et al. 1977; Muramatsu 1983). This interpretation has prompted studies to determine the causal mechanism for diurnal forcing of deep eyewall convection (Hobgood 1986).

The studies of Browner et al. (1977), Muramatsu (1983), and Lajoie and Butterworth (1984) considered the areal extent of clouds with equivalent blackbody cloud-top temperatures (T_{BB}) colder than a varying set of temperature thresholds. Steranka et al. (1984) examined the spatial variation of T_{BB} evolution by considering average T_{BB} within a group of annuli at varying distances from storm center. They divided a storm-centered disk with radius 888 km (8° lat) into eight annuli, each with a radial width of 111 km. The average T_{BB} in each annuli was based on 538 satellite images from 23 tropical cyclones that occurred over a 6-yr period. After stratifying by intensity, their averaged T_{BB} values were normalized to local standard time (LST) and placed into 1-h bins covering a 24-h period. Finally, a 3-h running mean was applied to their averaged values. The application of time series analyses to their composited T_{BB} dataset showed that 1) in hurricanes and tropical storms, a significant diurnal oscillation in T_{BB} exists and

Corresponding author address: Dr. James P. Kossin, Cooperative Institute for Research in the Atmosphere, Colorado State University, Fort Collins, CO 80523-1375.
E-mail: kossin@cira.colostate.edu

explains a large percentage of variance in each annulus; 2) in general, the diurnal oscillation is less significant and explains less variance in hurricanes than in tropical storms, particularly near the storm center; 3) within the outer annuli in tropical storms, a significant semidiurnal (12 h period) oscillation in T_{BB} exists, but the significance weakens considerably at inner radii and at all radii in hurricanes. In their study, significance was established against a white noise spectrum using a one-sided Fisher t test.

The present work extends, and sometimes challenges, the results of these previous studies of daily variability inferred from T_{BB} in tropical cyclones. Using a large IR dataset and best track information regarding storm center (described in section 2), Hovmöller-type diagrams of T_{BB} in individual storms are created (section 3a). These diagrams greatly facilitate the interpretation of the previous studies by succinctly capturing many of their results. Additionally, by considering storms on an *individual* basis, highly significant semidiurnal oscillations sometimes emerge that were not previously found, and diurnal oscillations that were previously noted are found to sometimes vanish entirely. In particular, results of time series analyses (section 3b) in a group of individual storms show that the diurnal oscillation of T_{BB} associated with the tropical cyclone cirrus canopy often becomes insignificant near the storm center, and is sometimes replaced by a highly significant semidiurnal oscillation.

The general absence of a significant diurnal oscillation of T_{BB} near the convective center of hurricanes suggests that the diurnal oscillation of cirrus canopies may not be physically linked to convection, as previously believed. In section 4a, an alternative mechanism based on radiative balance is proposed to explain the diurnal oscillation of the hurricane canopy. A mechanism based on local lapse-rate variability associated with the solar semidiurnal atmospheric tide S_2 is proposed in section 4b to explain the semidiurnal oscillation of T_{BB} above the central hurricane convection.

2. Data and method of analysis

The National Environmental Satellite, Data, and Information Service–Cooperative Institute for Research in the Atmosphere (NESDIS–CIARA) tropical cyclone infrared satellite imagery archive contains half-hourly, 4-km horizontal resolution, geostationary IR images of tropical cyclones that occurred since the onset of the 1995 hurricane season (Zehr 2000). The majority of archive images are from the Atlantic and eastern Pacific ocean basins and were captured by the east and west Geostationary Operational Environmental Satellites (GOES). As of December 2001, the archive contained over 50 000 images, yet it currently remains largely unexplored. An example of a typical image from the archive is shown in Fig. 1.

The present work combines the imagery from the

TABLE 1. Number of images used from the NESDIS/CIARA tropical cyclone archive for each of the 21 storms of 1999 (Atlantic storms Arlene to Lenny, and eastern Pacific storms Adrian to Irwin). Here, TS denotes a tropical storm and HU signifies that hurricane intensity was attained. The third column shows the time period spanned by the images.

Storm name	No. of images	Time period
TS Arlene	235	2145 UTC 11 Jun–1745 UTC 17 Jun
HU Bret	263	0015 UTC 18 Aug–2145 UTC 23 Aug
HU Cindy	555	0000 UTC 19 Aug–1515 UTC 31 Aug
HU Dennis	549	0015 UTC 24 Aug–1745 UTC 5 Sep
TS Emily	203	0015 UTC 24 Aug–1445 UTC 28 Aug
HU Floyd	515	0015 UTC 7 Sep–0915 UTC 17 Sep
HU Gert	502	1200 UTC 11 Sep–1815 UTC 23 Sep
TS Harvey	108	1715 UTC 19 Sep–0745 UTC 22 Sep
HU Irene	311	0015 UTC 12 Oct–0545 UTC 19 Oct
HU Jose	351	1745 UTC 17 Oct–1245 UTC 25 Oct
TS Katrina	223	0215 UTC 28 Aug–2145 UTC 31 Nov
HU Lenny	423	0015 UTC 13 Nov–2345 UTC 21 Nov
HU Adrian	157	0015 UTC 18 Jun–1130 UTC 21 Jun
HU Beatriz	378	0000 UTC 9 Jul–2330 UTC 16 Jul
TS Calvin	86	1500 UTC 25 Jul–0930 UTC 27 Jul
HU Dora	672	0015 UTC 6 Aug–2332 UTC 21 Aug
HU Eugene	440	0000 UTC 6 Aug–1700 UTC 15 Aug
TS Fernanda	218	0000 UTC 17 Aug–2030 UTC 21 Aug
HU Greg	204	0000 UTC 5 Sep–2330 UTC 9 Sep
HU Hilary	184	1600 UTC 17 Sep–2130 UTC 21 Sep
TS Irwin	133	0000 UTC 8 Oct–0330 UTC 11 Oct
Total No.	6710	

archive with the “best track” datasets for the North Atlantic and central and east Pacific basins. The best track datasets are maintained by the Tropical Prediction Center of the National Hurricane Center and contain 6-hourly storm center fixes (see Jarvinen et al. 1984 for more information). Cubic spline interpolation is used in the present work to interpolate the center fixes to the times of each image. Since daily variability will be considered in section 3, all times are converted from coordinated universal time (UTC) to local standard time using the best track interpolated longitude. The results presented in section 3 are based on storms that occurred in the Atlantic and eastern Pacific basins during the 1999 hurricane season (Table 1). This sample includes 12 named storms (8 hurricanes) from the Atlantic basin and 9 named storms (6 hurricanes) from the eastern Pacific basin.

With information regarding storm center, azimuthally averaged T_{BB} can be calculated at varying distances from the center, and Hovmöller-type diagrams (radius vs time) can be created. The Hovmöller diagrams comprise a set of individual time series in 4-km radial increments, and objective time series analyses can be performed at each radius. Since the storm center is not generally located at the center of each image, but traverses through the scene with time, azimuthal averaging was only performed along circles that were entirely contained in the image. It should be noted that there are a number of sources of possible errors related to the storm center information. These errors can, for example, result from

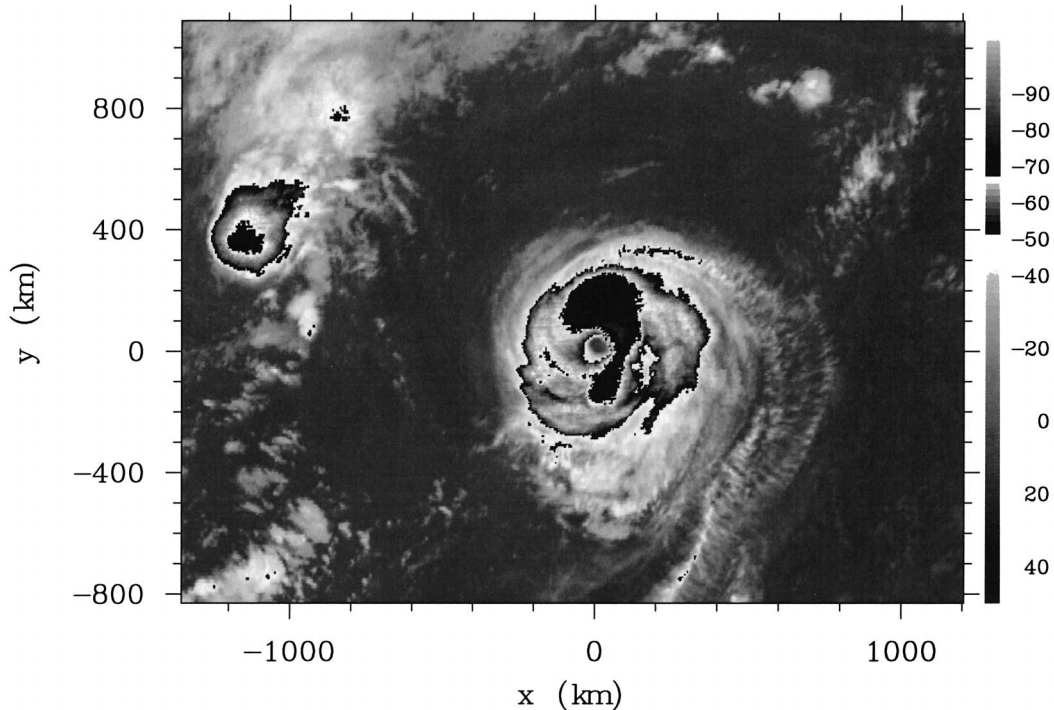


FIG. 1. Example of a full-scene image from the NESDIS/CIRA tropical cyclone IR imagery archive showing category 3 Atlantic Hurricane Alberto on 12 Aug 2000. The scene spans 2560 km (640 pixels) zonally and 1920 km (480 pixels) meridionally. As indicated on the label bar, the grayscale transitions from black to white three times as: 1) T_{BB} decreases from 50°C to -50°C, 2) T_{BB} decrease from -50°C to -65°C, and 3) T_{BB} decreases from -65°C to -110°C. The point $x = 0$, $y = 0$ corresponds to the best track storm center interpolated to the time of the image (35.9°N, 55.4°W).

1) less than perfect best track center fixes, 2) interpolation of the best track fixes, 3) differences between the storm center at the surface and at cloud top, as could be expected in a sheared environment, and 4) parallax due to the displacement of the storm center from satellite nadir. It is not expected that these errors should have a substantial effect on the results shown in section 3.

Spectral analyses of the time series were carried out using a standard lag-correlation method (Mitchell et al. 1966). Due to satellite eclipse periods (3 h or less) and other less predictable events, the data are not always uniformly spaced in time, and cubic spline interpolation was used to fill data-void periods. Because of the possible contamination of time series spectra by interpolation, the spectra discussed in section 3 were tested for consistency and robustness in a variety of ways, including tests using Lomb periodograms (Lomb 1976; Press et al. 1992). It was found that changes in the spectra due to interpolation were negligible in all cases. Prior to spectral analysis, each time series was truncated so that its fundamental period was an integer number of days. The truncated time series was then detrended and tapered. The results of the spectral analyses were tested for significance against a Markov (red noise) null continuum (Gilman et al. 1963). When highly significant spectral peaks associated with the 12- or 24-h-period

harmonics were identified, harmonic analyses were performed to ascertain the amplitude and phase of each harmonic. The highly significant spectral peaks were identified as having confidence levels greater than 99.99%. This strict requirement was deemed appropriate when considering the spectra in individual storms, where random oscillations are more likely than in large sample T_{BB} composites.

3. Results

a. Hovmöller diagrams

Representative Hovmöller diagrams are shown in Fig. 2 for the cases of eastern Pacific Hurricanes Beatriz and Dora, and Atlantic Hurricanes Bret and Floyd. Each image covers a different duration depending on the lifetime of each storm. The lifetime is determined by the time span of the best track data. As seen in Fig. 2, each storm has cold T_{BB} concentrated near the center ($r = 0$) during the earlier part of its lifetime. The appearance of the eye is clearly evident in each diagram as a region of warmer T_{BB} emerges suddenly in the central dense

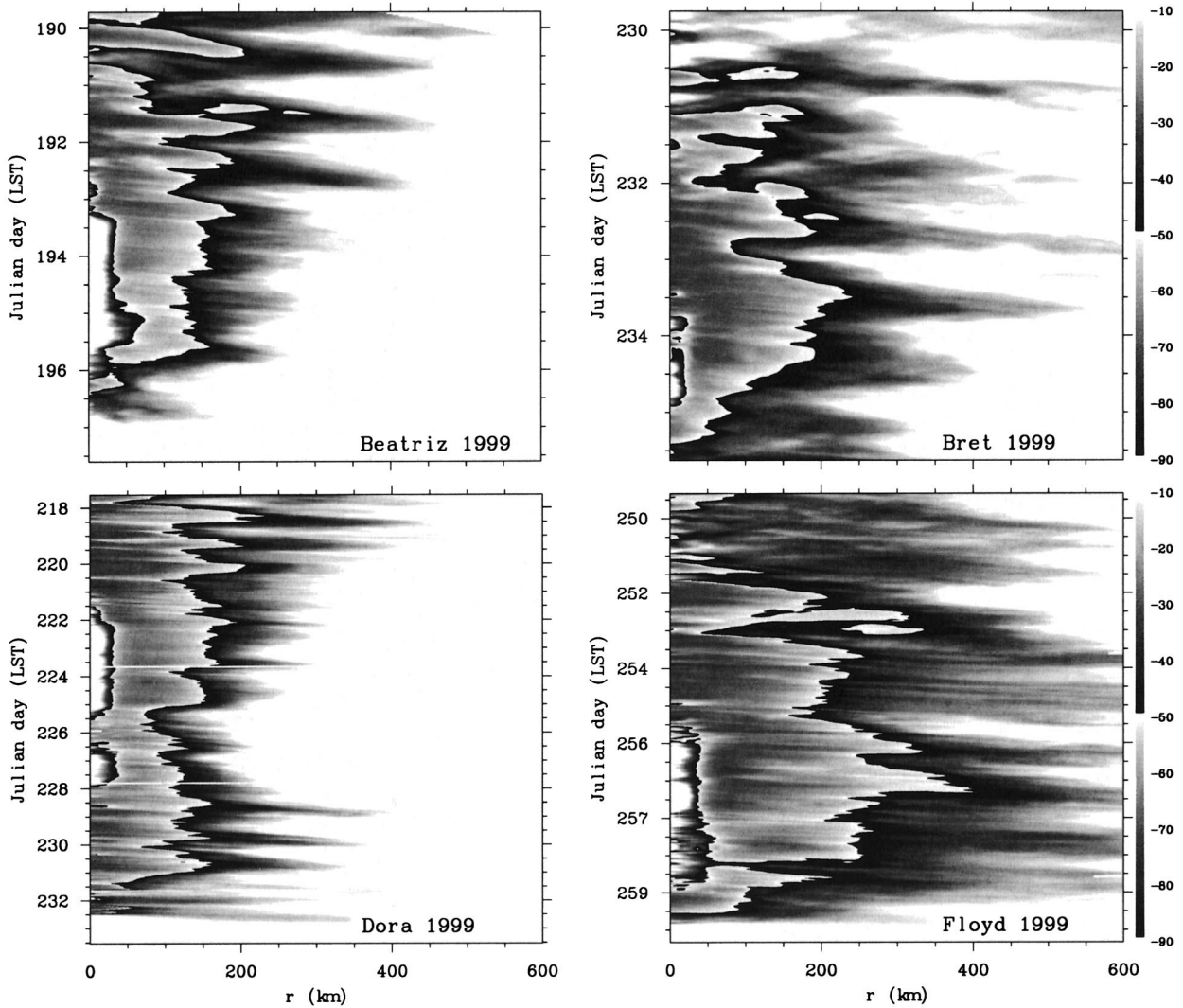


FIG. 2. Hovmöller (radius vs LST) diagrams of azimuthally averaged T_{BB} in eastern Pacific Hurricanes Beatriz and Dora, and Atlantic Hurricanes Bret and Floyd. Averages are with respect to interpolated best track center. Time, in Julian days, increases downward. The time span (vertical axis) is different for each storm. Values shown along the label bars are $^{\circ}\text{C}$.

overcast (CDO) at $r = 0$ with the coldest clouds (eye-wall) surrounding it.¹

Further casual scrutiny of the diagrams in Fig. 2 reveals the well-documented diurnal oscillation in T_{BB} outside the cold cloud tops of the central convective region. The cloud field in this region is dominated by the cirrus canopy above the storm and the periodic oscillations are largely induced by an oscillation in the horizontal areal extent of the canopy. As noted by Browner et al. (1977), the areal range of this oscillation is found to be inversely proportional to storm intensity. This can be seen most clearly in Fig. 2 in Beatriz, Dora, and Bret, but is not as obvious in Floyd. The reason for the inverse rela-

tionship between the areal range of the canopy oscillation and storm intensity is not well understood, but may be associated with a radial contraction of the descending branch of the hurricane secondary (transverse) circulation during intensification (Browner et al. 1977).

Although a significant amount of variation exists, the maximum areal coverage of the canopy often occurs near the time of local sunset, in agreement with the results of Browner et al. (1977) who noted an average maximum, based on three T_{BB} thresholds, at 1700 LST. Using T_{BB} thresholding methods, Muramatsu (1983) found the maximum areal extent of $T_{BB} \leq -70^{\circ}\text{C}$ to occur between 0600 and 0730 LST. For the ranges, $-70^{\circ}\text{C} < T_{BB} \leq -50^{\circ}\text{C}$, $-50^{\circ}\text{C} < T_{BB} \leq -30^{\circ}\text{C}$, and $-30^{\circ}\text{C} < T_{BB} \leq 0^{\circ}\text{C}$ the maximum was found to be 0900–1200 LST, 1500–1800 LST, and near 2100 LST, respectively. After detailed investigation of this “phase

¹ It should be noted that the appearance of the eye in the CDO does not necessarily coincide with the formation of the eye at lower levels in the storm.

lag," Muramatsu concluded that the times of maximum areal coverage are delayed when T_{BB} thresholds are increased or when the clouds considered are further from the storm center. Lajoie and Butterworth (1984) used similar thresholding methods to study tropical cyclones of the Australian region. They noted the maximum areal extent of $T_{BB} \leq -75^{\circ}\text{C}$, $T_{BB} \leq -65^{\circ}\text{C}$, and $T_{BB} \leq -55^{\circ}\text{C}$ to occur at 1800 LST, 1800 LST, and 2100 LST, respectively. Thus, while the specific results vary between the previous studies of Browner et al. (1977), Muramatsu (1983), and Lajoie and Butterworth (1984), the three studies all make the point that the time of maximum areal coverage of the canopy is systematically dependent on the T_{BB} considered, and typically occurs later for warmer thresholds. Using thresholding methods over large rectangular T_{BB} fields, the explanation for this systematic dependence can be difficult to determine. In support of the explanation hypothesized by Muramatsu (1983), the Hovmöller diagrams shown in Fig. 2 concisely demonstrate that this systematic dependence most likely results from the expansion and resultant thinning (and subsequent increase in T_{BB}) of the cirrus canopy.

It is of interest to note that Albright et al. (1985) found a similar systematic dependency between T_{BB} thresholds and areal coverage of cloudiness in the quiescent (i.e., devoid of tropical storms) tropical atmosphere. They found that clouds with tops in the -20° to -55°C range exhibited maximum coverage near local sunset, while clouds with tops colder than -65°C exhibited maximum coverage near local sunrise. They described this phase lag as a "downward delay," which they interpreted as follows:

...the picture emerges of a population of very deep clouds that increases in areal coverage during the night and reaches its peak near sunrise and of a second population of less deep clouds that increases rapidly around noontime, peaks near sundown and then diminishes in amount. . .

Thus their interpretation of the phase lag relies on the individual behaviors of two disparate cloud populations. This is a very different interpretation than the interpretation of the phase lag of the hurricane cirrus canopy described in the previous paragraph, in which the time of maximum cloudiness at different T_{BB} appears to depend entirely on the behavior of the cirrus canopy and not on the behavior of disparate cloud populations. Note that when a cirrus canopy is in place, satellite derived T_{BB} can give no information about other cloud populations that might exist below it. If we consider that deep convective clouds typically form cirrus anvils aloft, it seems quite plausible that the phase lag noted by Albright et al. (1985) could be alternatively interpreted solely in terms of expansion and resultant thinning (and subsequent increase in T_{BB}) of the cirrus anvils. The distinction between these two interpretations is an important one for understanding the general characteristics of tropical cloudiness, but a formal reex-

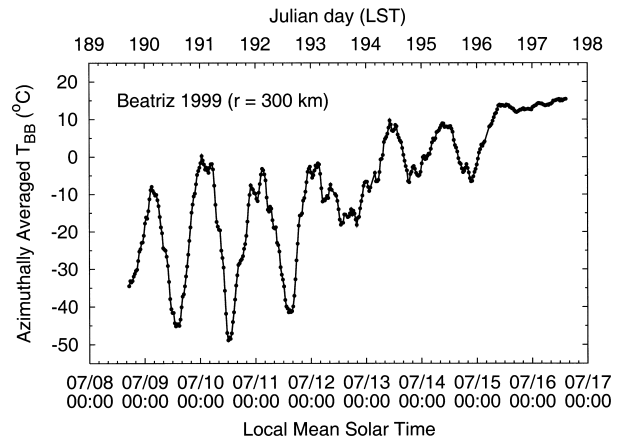


FIG. 3. Time series of azimuthally averaged T_{BB} in Hurricane Beatriz at $r = 300$ km. Time period is 8–17 Jul (Julian days 189–198).

amination of the results of Albright et al. (1985) lies beyond the scope of the present work, and is left here for future research.

b. Time series analyses

While the diurnal (24 h period) oscillations of the canopies over the storms in Fig. 2 are easily discernable outside the central convective regions, it is not immediately clear whether these oscillations are significant closer to the storm center. To study the evolution of cloudiness more objectively, and more completely, time series analyses were applied to the 21 Hovmöller diagrams associated with the full set of storms from 1999. Since each Hovmöller diagram is composed of 150 time series, each at a different radius from 4 to 600 km, 3150 time series were analyzed.

An example of a T_{BB} time series demonstrating the diurnal oscillation of the canopy above Hurricane Beatriz is shown in Fig. 3. As the cirrus canopy extends over the circular region at $r = 300$ km, local T_{BB} decreases significantly. During the earlier part of the time series, the diurnal range of T_{BB} is as high as 50°C . Beatriz became a hurricane on 11 July at around 0730 LST and intensified over the following 36 h, achieving maximum intensity around 1900 LST 12 July. After this time, T_{BB} at $r = 300$ km was higher on average, and the diurnal range decreased to around 17°C . The results of a spectral analysis performed on this time series are shown in Fig. 4 and clearly demonstrate the significance of the diurnal harmonic. There is also evidence of a weaker semidiurnal (12 h period) harmonic. A highly significant diurnal harmonic was present in Beatriz at all radii from 200 to 500 km. However, at all radii inside $r = 200$ km, the diurnal harmonic became insignificant and a highly significant semidiurnal harmonic emerged. An example is shown in Figs. 5 and 6, which show the T_{BB} time series for Beatriz at $r = 100$ km, and its spectrum. The lack of a significant diurnal harmonic is ev-

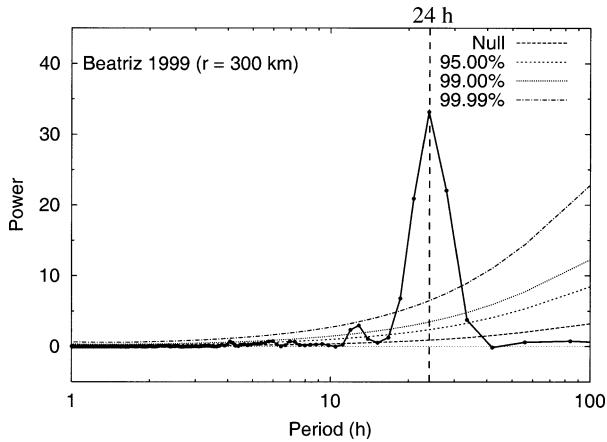


FIG. 4. Power spectrum associated with the time series shown in Fig. 3. The power is shown with respect to the periods of the harmonics, on a logarithmic scale, from 1 h (the Nyquist period) to 100 h. Dashed curved lines denote varying confidence levels. The diurnal (24-h period) oscillation is shown by the vertical dashed line.

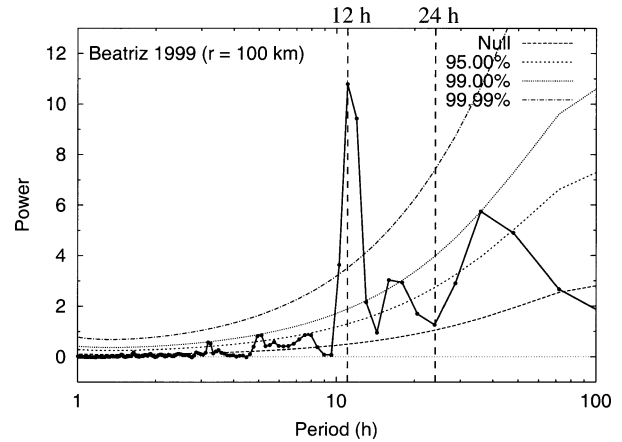


FIG. 6. Similar to Fig. 4 but for the time series shown in Fig. 5. The lack of a significant diurnal harmonic is clearly evident, but a highly significant semidiurnal harmonic is present.

ident, and a semidiurnal harmonic dominates the spectrum. The phase of the semidiurnal harmonic (time of maximum T_{BB}) is around 1000 and 2200 LST and is thus nearly in phase with the solar semidiurnal atmospheric tide (S_2), which has a maximum around 0945 and 2145 LST [see e.g., Whiteman and Bian (1996), Dai and Wang (1999), and references cited therein]. Thus T_{BB} near the convective region of the storm center

is coldest when the S_2 pressure oscillation is a minimum, that is, around 0400 and 1600 LST. The range associated with the semidiurnal harmonic of the total T_{BB} time series in Beatriz was $\sim 7^\circ\text{C}$. During the earlier part of the time series, the semidiurnal range of T_{BB} in Beatriz was as large as $\sim 20^\circ\text{C}$.

The results of the time series analyses of all 21 storms at all radii are summarized in Fig. 7. The thick solid (dashed) lines span all radii where highly significant diurnal (semidiurnal) oscillations were found. It is clear

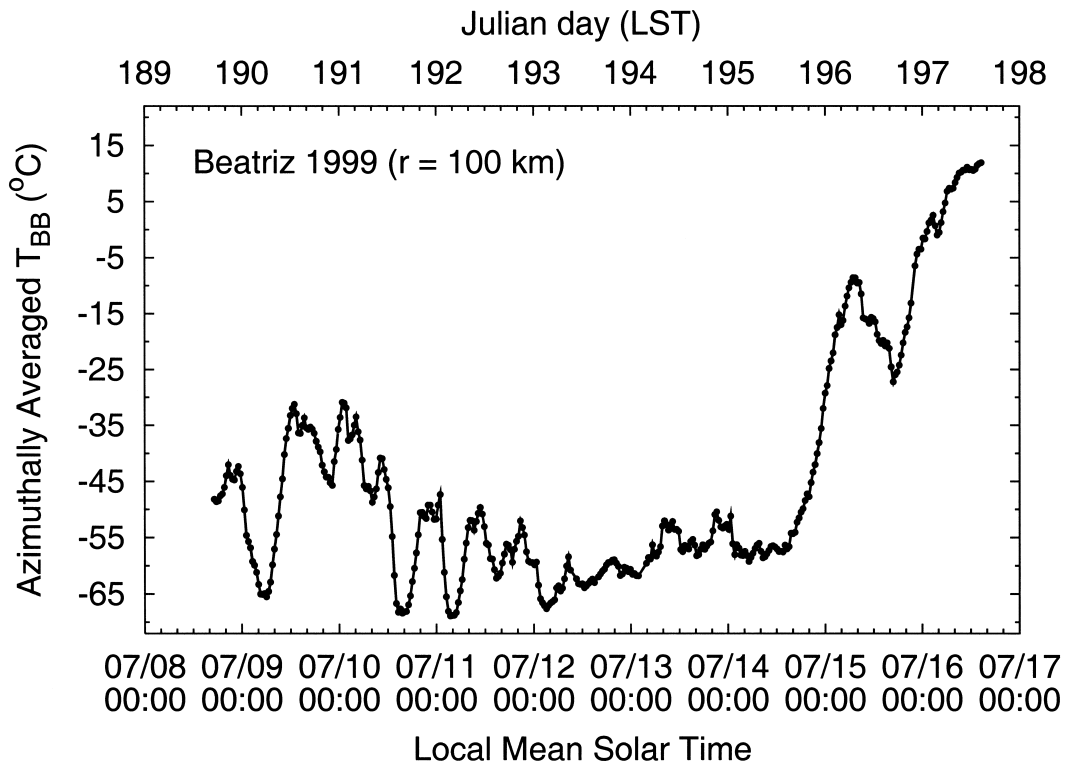


FIG. 5. Similar to Fig. 3 but for $r = 100$ km.

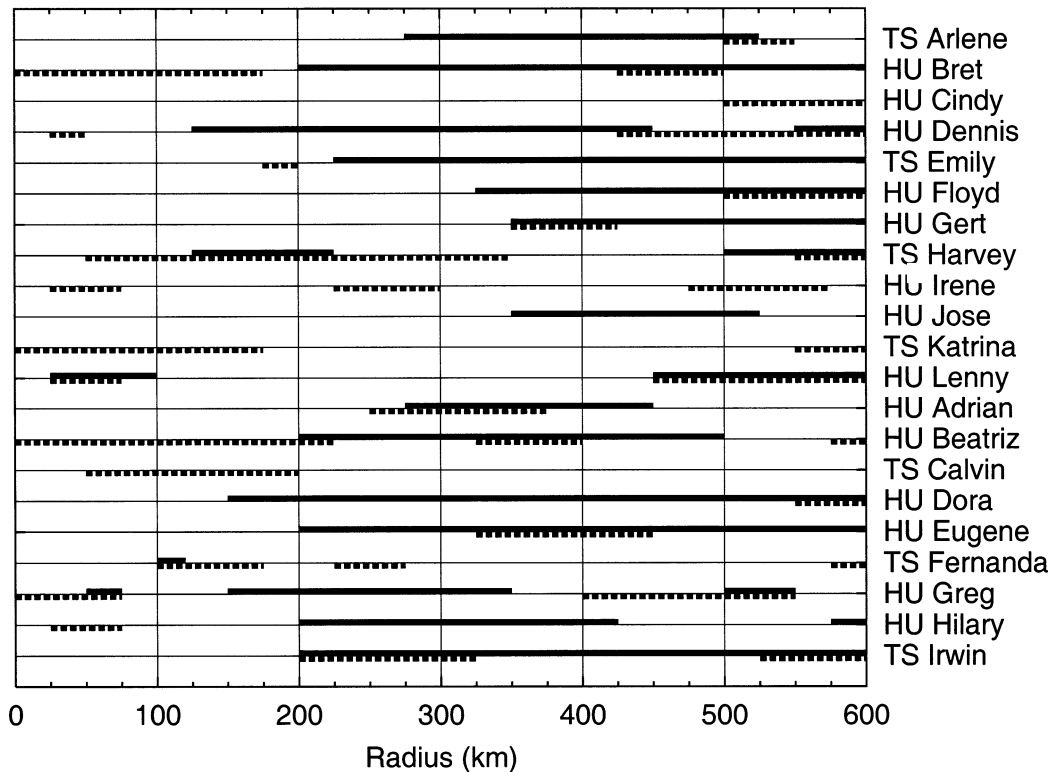


FIG. 7. Results of time series analyses at all radii in the 21 storms listed in Table 1. The thick solid (dashed) lines span all radii where the diurnal (semidiurnal) harmonics were significant at confidence levels greater than 99.99%.

that most of the 21 storms exhibit a highly significant diurnal oscillation within some annulus between 0 and 600 km. The only exceptions are Hurricanes Cindy and Irene, and Tropical Storms Katrina and Calvin. The significant diurnal oscillations are more often found beyond $r = 300$ km. For example, 16 of the 21 storms have significant diurnal oscillations in some annulus beyond $r = 300$ km. This is the region where the T_{BB} field is dominated by the cirrus canopy. However, within annuli that are closer to the convective region near the storm center ($0 \leq r \leq 200$ km), most storms (15 out of 21) do not exhibit a significant diurnal oscillation in T_{BB} . Within the innermost 100-km annulus, only two of the storms exhibited diurnal T_{BB} oscillations. In contrast, 10 of the storms exhibited highly significant semidiurnal oscillations within this annulus. The semidiurnal range of T_{BB} within this annulus is typically $\sim 10^\circ\text{C}$. The semidiurnal oscillations are found within all annuli, but are especially prevalent within the innermost and outermost regions. The semidiurnal oscillation in the outer region was also noted by Steranka et al. (1984). In the present study, the phase of the semidiurnal harmonics is consistently around 1000 LST regardless of distance from storm center. This result strongly suggests a physical connection between T_{BB} and the amplitude of the S_2 pressure perturbation. Speculation on a possible explanation for such a connection will be discussed in the following section.

As discussed in section 2, highly significant harmonics are identified as having confidence levels greater than 99.99%. The results shown in Fig. 7 would not change substantially if confidence level requirements were reduced to 95%, except for a slight radial spreading of the solid and dashed lines. In other words, diurnal and semidiurnal spectral peaks that are significant at the 95% confidence level are also generally significant at the 99.99% confidence level or higher. This is evident in Figs. 4 and 6 where the spectral peaks are well above the 99.99% confidence level. Spectral peaks with periods other than 12 and 24 h also occasionally emerge from the time series analyses, but the periods of these peaks are generally not consistent among the 21 storms. For example, there are spectral peaks with periods ~ 18 h and ~ 36 h seen in Fig. 6, but these peaks are not typically found in other storms. Furthermore, the a priori significance testing applied to the diurnal and semidiurnal harmonics is not appropriate for other periods since there is no a priori expectation of finding such spectral peaks. A few of the storms exhibited powerful spectral peaks at higher frequencies (periods between 7 and 10 h), particularly in annuli with smaller radii ($r < 100$ km). Again, the periods of these peaks were not robust among the different storms, but their presence is intriguing. Browner et al. (1977) noted the presence of a 4-h-period oscillation in their study, but no such high-frequency oscillations were found in the present work. Thus it appears that the evo-

lution of *typical* hurricane cloudiness exhibits no significant regular oscillations other than diurnal and semidiurnal oscillations.

4. Discussion

a. A hypothesized mechanism for the diurnal oscillation of the hurricane canopy

The results of section 3 suggest the need for a revised hypothesis to explain the mechanisms responsible for the daily variation of hurricane cloudiness. The well-documented diurnal cycle of the hurricane cirrus canopy has conventionally been thought to be forced by a diurnal cycle in the convection in the eyewall and surrounding spiral bands (e.g., Browner et al. 1977; Muramatsu 1983). This previously suggested link between convection and the areal extent of the canopy is apparently based on an expected increase in the areal extent of the upper-level hurricane outflow, associated with an increase in convection. Under the observationally based assumption that convection in general tropical oceanic regions often exhibits an early morning maximum, the previous studies argue that the maximum areal extent of the canopy (often observed around local sunset) lags the convective maximum because the cirrus generated at the storm center takes 12–18 h to reach the canopy edge, based on some mean upper-level outflow (radial wind) speed (see also Merritt and Wexler 1967). Motivated by the results of these previous observational studies, Hobgood (1986) argues that hurricane convection is forced by a diurnal oscillation of lapse rates resulting from cloud-top radiative cooling.

If the results of these previous studies by Browner et al. (1977), Muramatsu (1983), and Hobgood (1986) were typically true, we might expect to find significant diurnal oscillations in the convective regions as well as the outer regions where the canopy dominates the cloud field. However, as shown in Fig. 7, while most storms exhibit diurnal oscillations in their canopies, very few exhibit these oscillations in the cloud tops over their convective centers. Thus the central or eyewall convection may not be diurnally forced as previously believed.² It should be noted that convection occurring within the hurricane spiral bands may also at times play an important role in the maintenance of the cirrus canopy. Can a diurnal oscillation in the convection in the spiral bands be implicated as the cause for the diurnal oscillation of the canopy? The evolution of Hurricane Dora may provide an answer to this question. During the mature stages of its lifetime, Dora transitioned to a quasi-steady state in which virtually all spiral band features vanished. During this period of no spiral bands, the diurnal oscillation of the cirrus canopy remained

pronounced. Thus it does not appear that a diurnal oscillation in the convection in the spiral bands can be implicated as the cause for the diurnal oscillation of the canopy.

If the diurnal variability of the hurricane canopy is not forced by a similar oscillation in convection, then another mechanism needs to be identified. A hypothesized mechanism is offered here: Consider the general model for the hurricane secondary (transverse) circulation in which low-level convergence results in upward motion near the storm center. The deep central updrafts result in divergence (outflow) aloft. This transverse circulation is completed by a descending branch where the outflowing mass begins its descent to the surface. The upper-level outflow carries convective cloud particles outward as glaciation occurs. This creates the cirrus canopy. Now consider the effects of a cessation of incident solar energy on the canopy region. Longwave cooling in the absence of short wave warming results in net cooling locally. The atmospheric response to this net cooling is manifested as an increase in local subsidence. This subsidence is expected to be greater in clear (warm T_{BB}) versus cloudy (cold T_{BB}) regions (see e.g., Gray and Jacobson 1977). The Hovmöller diagrams of Fig. 2 show that T_{BB} of the canopy increases with radius, and thus radiatively driven subsidence (and resulting warming) may increase with radius. The radial dependence of the warming of the subsiding air would manifest as an apparent “shrinking” of the areal extent of the canopy. Increased sublimation of ice particles within the subsiding air may also play a role in the shrinking of the canopy. Based on this hypothesized mechanism, the shrinking would be expected to begin near local sunset and end near local sunrise, in agreement with the evolutions shown in Fig. 2. Note that this hypothesis relies on convection to create and maintain the canopy, but the diurnal oscillation of the canopy is dissociated from the convection.

Figure 8 displays this hypothesized diurnal oscillation of an idealized hurricane transverse circulation. During the 12-h period following 1800 LST, the outflowing branch of the transverse circulation tilts downward as the air in which the outflow is embedded subsides due to local net radiative cooling. After sunrise at 0600 LST, incoming shortwave radiation balances outgoing longwave radiation, local subsidence decreases, and the outflowing air of the transverse circulation ceases to be drawn downward. An example of this simple conceptual model can be easily constructed. Assume that the azimuthally averaged T_{BB} radial profile at $t = 1800$ LST is given by the linear relationship

$$T_{BB}(r, t = 1800 \text{ LST}) = T_{BB}^{\text{center}} + \frac{T_{BB}^{\text{outer}} - T_{BB}^{\text{center}}}{r_{\text{outer}}}r, \quad (1)$$

where T_{BB}^{center} and T_{BB}^{outer} are brightness temperatures at $r = 0$ and $r = r_{\text{outer}}$ respectively. Now assume that the canopy region exists between r_{inner} and r_{outer} and the evo-

² Of course, such a hypothesis necessarily rests on the assumption that the behavior of convective clouds can be correctly inferred from satellite derived T_{BB} .

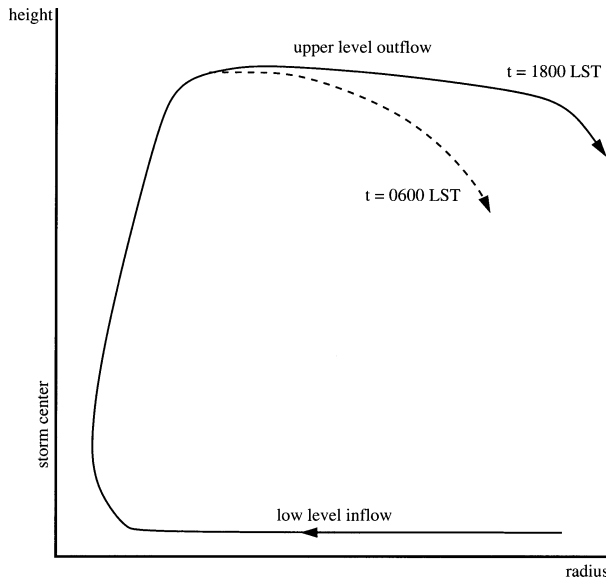


FIG. 8. Schematic showing a hypothesized diurnal oscillation of the hurricane transverse circulation. At $t = 1800$ LST, the outward radial extent of the outflow branch is maximum and the cirrus canopy has maximum areal extent. During the following 12 h, subsidence draws the outflow branch downward, resulting in a warming and subsequent apparent “shrinking” of the cirrus canopy.

lution of the azimuthally averaged vertical displacement of the canopy (from its position at $t = 1800$ LST), between r_{inner} and r_{outer} is given by

$$H(r, t) = \frac{H_{max}}{2} \frac{r - r_{inner}}{r_{outer} - r_{inner}} \left\{ 1 - \cos \left[\frac{2\pi(t - 18)}{24} \right] \right\}, \quad (2)$$

where t is measured in hours from 0000 LST, and H_{max} is the maximum vertical displacement of the canopy at $r = r_{outer}$ (occurring daily at 0600 LST). Equation (2) describes a harmonic oscillator with 24-h period and minimum at $t = 18$ h, and a linear dependence on radius. If the local lapse rate of the canopy region is given by Γ , then the evolution of the azimuthally averaged T_{BB} field can be idealized as

$$T_{BB}(r, t) = \begin{cases} T_{BB}(r, t = 1800 \text{ LST}) & 0 \leq r \leq r_{inner}, \\ T_{BB}(r, t = 1800 \text{ LST}) + \Gamma H(r, t) & r_{inner} \leq r \leq r_{outer}. \end{cases} \quad (3)$$

An example of the purely diurnal T_{BB} evolution calculated from (3) is shown in Fig. 9 in the form of a Hovmöller diagram and bears a strong resemblance to the diurnal features in the canopy regions of the storms displayed in Fig. 2. Thus, the diurnal oscillation of the cirrus canopies shown in Fig. 2 can be fairly well explained using a very simple model in the complete absence of a diurnal oscillation in convection. The model is based on the assumption that the amount of nighttime radiatively driven subsidence in the canopy region be-

yond the central convective region increases with increasing distance from storm center.

b. A hypothesized mechanism for the semidiurnal oscillation in the hurricane central convective region

The fairly common presence of a significant semidiurnal T_{BB} oscillation in the central convective regions of hurricanes poses the question of what might be causing it. This semidiurnal oscillation is consistently in phase with the solar semidiurnal atmospheric tide S_2 . In the general tropical atmosphere, possible physical connections between cloudiness and S_2 have been hypothesized by a number of previous authors. Brier and Simpson (1969) postulated a dynamic mechanism where local changes in low-level convergence are caused by the migration of the pressure tide, and they argued that the increase in convergence then leads to an increase in cloudiness. Deser and Smith (1998) pointed out that the time of maximum surface wind convergence actually lags the maximum of the well documented semidiurnal rainfall oscillation. Rainfall variability is associated with variability of deep convection. Additionally, they noted that the deep layer convergence associated with the migration of S_2 should not appreciably change local vertical velocity (see also Lindzen 1967). Based on these two points, they argued that there is not a clear link between S_2 and rainfall (and cloudiness) variability through a mechanism based on convergence variability.

A new mechanism, linking the vertical structure of S_2 and local cloudiness, is hypothesized here: The thermal tide theory of Lindzen (1967) describes S_2 as vertically uniform, but a recent study by Chen et al. (2001) found significant vertical variability of the S_2 pressure perturbation using observations from two stations at different elevations on the island of Taiwan. Harris et al. (1962) combined 6-hourly rawinsonde data from different years to construct a 3-hourly rawinsonde dataset. Using this 3-hourly data, they considered the vertical structure of the semidiurnal oscillation of wind, pressure, and temperature associated with S_2 . They found small, but measurable, vertical variations of the amplitude and phase of the pressure oscillation in the troposphere. Thus, there appears to be vertical structure of the pressure perturbation associated with S_2 , but the details are currently not well understood. Perhaps more illuminating is the response of local lapse rates to local variations in pressure caused by S_2 . Regardless of whether the S_2 pressure perturbation has vertical structure, the local temperature response to the pressure perturbation can be expected to exhibit vertical structure since local atmospheric density is not vertically uniform. If local temperature perturbations associated with S_2 have vertical structure, then local lapse rates should oscillate semidiurnally. In support of this idea, a semidiurnal oscillation of local lapse rates, associated with S_2 , can be deduced from the temperature soundings con-

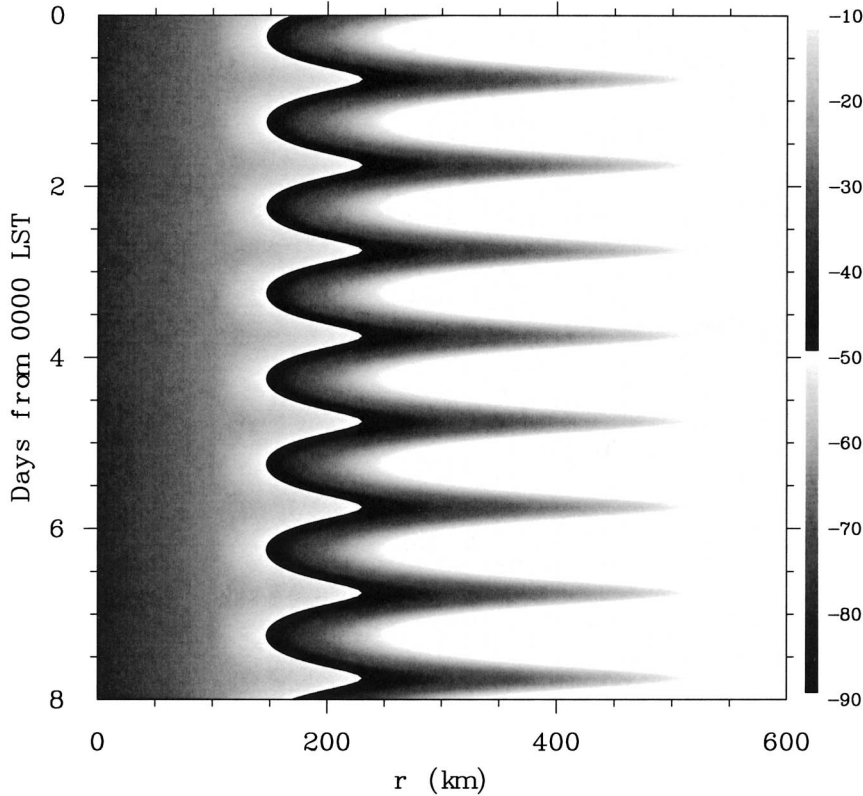


FIG. 9. Hovmöller (radius vs LST) diagram showing an idealized diurnal T_{BB} oscillation based on the hypothesized evolution given by Eq. (3), using $T_{BB}^{center} = -80^{\circ}\text{C}$, $T_{BB}^{outer} = 0^{\circ}\text{C}$, $r_{outer} = 600$ km, $r_{inner} = 100$ km, $\Gamma = 10^{\circ}\text{C km}^{-1}$, and $H_{max} = 8$ km. The diurnal behavior is similar to the diurnal behavior observed in the cirrus canopies of hurricanes, as shown in Fig. 2. For easier comparison with the diurnal features in Fig. 2, the number of days spanned along the ordinate was chosen to be similar to Beatriz (top-left of Fig. 2).

structed by Harris et al. (1962; shown in their Table 3). The lapse rates vary through a deep layer of the troposphere, and although the lapse-rate variation is fairly small as calculated from the annual mean values of Harris et al. (1962), the maximum destabilization occurs at 0400 and 1600 LST and is thus physically consistent with the results of this study that suggest a local increase in cloud heights around 0400 and 1600 LST.

5. Concluding remarks

Using the NESDIS/CIRA tropical cyclone infrared imagery archive, combined with best track center fix information, the daily variability of azimuthally averaged T_{BB} in tropical storms and hurricanes was considered. Many features of the well-documented diurnal oscillation of the cirriform canopy above the storms were succinctly captured with the use of Hovmöller diagrams. The diurnal oscillation is induced by the variability of the areal extent of the canopy. This has been previously believed to be caused by a diurnal oscillation in the deep convection near the hurricane center, and within the spiral bands. However, few storms in the present

study exhibited diurnal oscillations in T_{BB} above their central convective regions. This result suggests that the deep central convection may not be diurnally forced and the canopies might be forced by another mechanism. This mechanism was hypothesized to rely on the spatial structure of radiatively driven subsidence in the region of the cirrus canopy.

While few storms exhibited diurnal oscillations in T_{BB} above their central convection, a number of storms exhibited highly significant semidiurnal variability there. Semidiurnal oscillations were found at all distances from the storm centers, but were particularly common near the center and beyond the cirrus canopies. The phase of these oscillations were consistently in phase with the solar semidiurnal atmospheric tide (S_2), and the central cloud tops were found to be coldest around 0400 and 1600 LST. This suggests that a physical connection between S_2 and cold cloud tops exists, but the mechanism is as yet unknown. A hypothesis for this mechanism was suggested, based on the possible presence of a semidiurnal oscillation of local lapse rates associated with S_2 .

Acknowledgments. The author would like to thank his colleagues at CIRA and Colorado State University, particularly John Knaff, Ray Zehr, Mark DeMaria, Wayne Schubert, Dick Johnson, Paul Ciesielski, Stan Kidder, Don Hillger, Philip Gabriel, Tristan L'Ecuyer, Tom Vonder Haar, Dave Thompson, and Rick Taft, for their participation in many helpful discussions. The original manuscript benefited greatly from comments made by Dan Cecil and Elizabeth Ritchie. This work was supported by NOAA Grant NA67RJ0152.

REFERENCES

- Albright, M. D., E. E. Recker, R. J. Reed, and R. Dang, 1985: The diurnal variation of deep convection and inferred precipitation in the central tropical Pacific during January–February 1979. *Mon. Wea. Rev.*, **113**, 1663–1680.
- Brier, G. W., and J. Simpson, 1969: Tropical cloudiness and rainfall related to pressure and tidal variations. *Quart. J. Roy. Meteor. Soc.*, **95**, 120–147.
- Browner, S. P., W. L. Woodley, and C. G. Griffith, 1977: Diurnal oscillation of the area of cloudiness associated with tropical storms. *Mon. Wea. Rev.*, **105**, 856–864.
- Chen, T.-C., M.-C. Yen, and S. Schubert, 2001: Diurnal variation of pressure-heights: A vertical phase shift. *J. Climate*, **14**, 3793–3797.
- Dai, A., and J. Wang, 1999: Diurnal and semidiurnal tides in global surface pressure fields. *J. Atmos. Sci.*, **56**, 3874–3891.
- Deser, C., and C. A. Smith, 1998: Diurnal and semidiurnal variations of the low-level wind field over the tropical Pacific Ocean. *J. Climate*, **11**, 1730–1748.
- Gilman, D. L., F. J. Fuglister, and J. M. Mitchell Jr., 1963: On the power spectrum of “red noise.” *J. Atmos. Sci.*, **20**, 182–184.
- Gray, W. M., and R. W. Jacobson, 1977: Diurnal variation of deep cumulus convection. *Mon. Wea. Rev.*, **105**, 1171–1188.
- Harris, M. F., F. G. Finger, and S. Teweles, 1962: Diurnal variation of wind, pressure, and temperature in the troposphere and stratosphere over the Azores. *J. Atmos. Sci.*, **19**, 136–149.
- Hobgood, J. S., 1986: A possible mechanism for the diurnal oscillation of tropical cyclones. *J. Atmos. Sci.*, **43**, 2901–2922.
- Jarvinen, B. R., C. J. Neumann, and M. A. S. Davis, 1984: A tropical cyclone data tape for the North Atlantic Basin, 1886–1983: Contents, limitations and uses. NOAA Tech. Memo. NWS NHC 22, NOAA/National Hurricane Center, Miami, FL, 21 pp. [Available from NOAA/Tropical Prediction Center, 11691 S.W. 17th St., Miami, FL 33165-2149.]
- Lajoie, F. A., and I. J. Butterworth, 1984: Oscillation of high-level cirrus and heavy precipitation around Australian region tropical cyclones. *Mon. Wea. Rev.*, **112**, 535–544.
- Lindzen, R. S., 1967: Thermally driven diurnal tide in the atmosphere. *Quart. J. Roy. Meteor. Soc.*, **93**, 18–42.
- Lomb, N. R., 1976: Least-squares frequency analysis of unequally spaced data. *Astrophys. Space Sci.*, **39**, 447–462.
- Merritt, E. S., and R. Wexler, 1967: Cirrus canopies in tropical storms. *Mon. Wea. Rev.*, **95**, 111–120.
- Mitchell, J. M., Jr., B. Dzerdzevskii, H. Flohn, W. L. Hofmeyr, H. H. Lamb, K. N. Rao, and C. C. Wallen, 1966: Climatic Change. WMO Tech. Note 79, Geneva, Switzerland, 79 pp.
- Muramatsu, T., 1983: Diurnal variations of satellite-measured T_{BB} areal distribution and eye diameter of mature typhoons. *J. Meteor. Soc. Japan*, **61**, 77–89.
- Press, W. H., S. A. Teukolsky, W. T. Vetterling, and B. P. Flannery, 1992: *Numerical Recipes in Fortran 77*. Cambridge University Press, 963 pp.
- Steranka, J., E. B. Rodgers, and R. C. Gentry, 1984: The diurnal variation of Atlantic Ocean tropical cyclone cloud distribution inferred from geostationary satellite infrared measurements. *Mon. Wea. Rev.*, **112**, 2338–2344.
- Whiteman, C. D., and X. Bian, 1996: Solar semidiurnal tides in the troposphere: Detection by radar profilers. *Bull. Amer. Meteor. Soc.*, **77**, 529–542.
- Zehr, R. M., 2000: Tropical cyclone research using large infrared image data sets. *Proc. 24th Conf. on Hurricanes and Tropical Meteorology*. Fort Lauderdale, FL, Amer. Meteor. Soc. 486–487.